

# Hirshfeld surface analysis, interaction energy calculations and *in silico* anti-SARS-CoV-2 potentials of metal (II) 3,4-dimethoxybenzoate with nicotinamide complexes

Füreyra Elif ÖZTÜRKKAN<sup>1\*</sup>, Afşin Ahmet KAYA<sup>2</sup>, Elif ÇELENK KAYA<sup>2</sup>

<sup>1</sup>Kafkas University, Department of Chemical Engineering, Kars, 36100, Türkiye

<sup>2</sup>Ondokuz Mayıs University, Department of Property Protection and Safety, Samsun, Türkiye

Geliş Tarihi (Received Date): 12.11.2022

Kabul Tarihi (Accepted Date): 29.05.2023

## Abstract

*In this study, types of the intermolecular interactions, the intermolecular interaction energies, void analysis of diaquabis(3,4-dimethoxybenzoate)bis(nicotinamide)zinc(II) dihydrate (Complex 1), diaquabis(3,4-dimethoxybenzoate)bis(nicotinamide)nickel(II) dihydrate (Complex 2), diaquabis(3,4-dimethoxybenzoate)bis(nicotinamide)cobalt(II) dihydrate (Complex 3), whose crystal structures were characterized before, were investigated with the help of the CrystalExplorer program (Version 21.5). It has been determined that H···H, H···O/O···H, H···C/C···H, H···N/N···H, C···C, C···O/O···C, O···O, and C···N/N···C interactions are intermolecular interactions that contribute to the Hirshfeld surface of the complexes. According to the results of the interaction energy analysis calculated with the help of B3LYP/6-31G(d,p), B3LYP/6-31G(d), B3LYP/3-21G, HF/6-31G(d,p), HF/6-31G(d), HF/3-21G, DFT/6-31G(d,p), DFT/6-31G(d), DFT/3-21G, MP2/6-31G(d,p), MP2/6-31G(d), MP2/3-21G basis sets, the major amount of the total energy is contributed by electrostatic and polarization energies. The interactions between Complexes 1-3 and the main protease enzyme and the spike protein of Omicron variant of the SARS-CoV-2 were investigated by Molecular docking studies. It was determined that complexes 1-3 and the main protease enzyme and the spike protein of Omicron variant of the SARS-CoV-2 interact via attractive charges, hydrogen bonding, electrostatic contacts, and hydrophobic interactions. According to the obtained results, further in vivo/in vitro studies are recommended for complex 3. The results determined as a result of interaction energy analysis and molecular docking studies show that the hydrogen bonds formed by the hydrogen bond donor/acceptor groups in the structure of the complexes are an important factor in both the stability of the crystal package and inhibition of important enzymes of SARS CoV-2.*

**Keywords:** 3,4-Dimethoxybenzoic acid, transition metal complexes, Hirshfeld surface analysis, non-covalent interactions, molecular docking, SARS CoV-2.

## Metal (II) 3,4-dimetoksibenzoatın nikotinamid komplekslerinin Hirshfeld yüzey analizi, etkileşim enerjisi hesaplamaları ve *in silico* anti-SARS-CoV-2 potansiyelleri

### Öz

*Bu çalışmada, kristal yapıları daha önce karakterize edilmiş olan metal (II) 3,4-dimetoksibenzoatın nikotinamid komplekslerinin moleküllerarası etkileşim türleri, moleküllerarası etkileşim enerjileri ve boşluk analizi CrystalExplorer programı (Versiyon 21.5) yardımıyla incelenmiştir. H...H, H...O/O...H, H...C/C...H, H...N/N...H, C...C, C...O/O...C, O...O ve C...N/N...C etkileşimleri, komplekslerin Hirshfeld yüzeyine katkıda bulunan moleküller arası etkileşimlerdir. Hesaplanan etkileşim enerjisi analizi sonuçlarına göre, toplam enerjiye en önemli katkıyı elektrostatik ve polarizasyon enerjileri sağlamaktadır. Çalışmada ayrıca, kompleks 1-3 ile SARS CoV-2'nin ana proteaz enzimi ve Omicron varyantının spike proteini arasındaki etkileşimler Moleküler docking çalışmaları ile incelenmiştir. Kompleks 1-3'ün, yükler arası çekim kuvvetleri, hidrojen bağı, elektrostatik ve hidrofobik etkileşimler yoluyla SARS-CoV-2'nin ana proteaz enzimi ve Omicron varyantının spike proteini ile etkileşime girdiği belirlenmiştir. Elde edilen sonuçlara göre özellikle kompleks 3 için ileri in vivo/in vitro çalışmalar önerilmektedir. Etkileşim enerjisi analizi ve moleküler docking çalışmaları sonucunda belirlenen sonuçlar komplekslerin yapısında bulunan hidrojen bağı donör akseptör gruplar vasıtasıyla oluşan hidrojen bağlarının gerek kristal paketin kararlılığına gerekse SARS CoV-2'nin önemli enzimlerini inhibe etmede önemli birer faktör olduğunu göstermektedir.*

**Anahtar Kelimeler:** 3,4-Dimetoksibenzoik asit, geçiş metal kompleksleri, Hirshfeld yüzey analizi, kovalent olmayan etkileşimler, moleküler docking, SARS CoV-2.

### 1. Introduction

Computation, together with experiment and theory, has been characterized as the cornerstone of scientific investigation. Computation helps scientists to simulate realistic problems for which there are no analytical answers and to answer issues that are difficult to solve experimentally. Computational modeling is broadly applied in organic, physical, biological, material science, and medicinal research in chemistry [1, 2]. Fundamental knowledge and understanding of the structures, features, and chemical reactivity of molecules are gained through computational and theoretical chemistry. Theoretical calculations are currently crucial in many areas of chemical research and development as a result [3].

Hirshfeld surfaces are named after F.L. Hirshfeld, who proposed an extension of describing a molecule in a crystal with a "shareholder allocation" scheme to describe atoms in molecules. Over the past 10 years, the importance of evaluating molecular crystal structures using methods that are based on Hirshfeld surfaces has increased [4]. It is also helpful to determine intermolecular interactions using the Hirshfeld surface while maintaining the whole-molecule approach basis [5, 6]. Intermolecular interactions in

crystal structures can be easily analyzed and visualized utilizing Hirshfeld surface analysis in CrystalExplorer software [7].

Every day, new protein and nucleic acid structures are discovered, and new ones are added to Molecular Docking studies for drug development. In current drug design, molecular docking is routinely employed to investigate drug-target interactions. Small ligands with computer-generated 3D structures are placed into receptor structures with the help of Molecular Docking in a range of orientations, conformations, and placements. In this way, some predictions can be made for drug research before some time-consuming, challenging, and expensive experiments are carried out [8, 9]. Severe acute respiratory syndrome-coronavirus-2 (SARS-CoV-2) coronavirus disease, 2019 (COVID-19), has caused a worldwide pandemic that continues to threaten many lives worldwide. According to the findings of many studies, coronavirus variants are responsible for the increased infectivity, efficacy, and severity of the disease. Numerous investigations have revealed that when the SARS CoV-2 variants change, the Spike Receptor-Binding Domain (RBD) improves its affinity for the angiotensin-converting enzyme 2 (ACE2) receptor. Considering the effects on humanity, therapeutic treatment of this disease is a necessity. However, drug treatment, which is a common problem of many viral diseases, is also valid for this disease. The importance of computational research emerges when the duration of drug research and development studies is taken into account [10–12]. The COVID-19 main protease enzyme (Mpro) plays a vital role in viral replication, translation, and transcription processes. Mpro is, therefore, a potential pharmacological target for the creation of novel COVID-19 therapies [13, 14]. Studies on the drug potential of SARS CoV-2 are limited. So, it is important to know the effects of drug candidate compounds on various variants. For this purpose, in this study, we determined the non-covalent interactions of diaquabis(3,4-dimethoxybenzoate)bis(nicotinamide)zinc(II) dihydrate (Complex 1), diaquabis(3,4-dimethoxybenzoate)bis(nicotinamide)nickel(II) dihydrate (Complex 2), diaquabis(3,4-dimethoxybenzoate)bis(nicotinamide)cobalt(II) dihydrate complexes (Complex 3) with the help of Hirshfeld surface analysis. To determine the anti-SARS-CoV-2 potential, interactions with these complexes and the main protease enzyme of SARS-CoV-2 and the spike protein of Omicron variant of SARS-CoV-2 were examined.

## 2. Materials and methods

### 2.1. Materials

Crystal structure of diaquabis(3,4-dimethoxybenzoate)bis(nicotinamide)zinc(II) dihydrate (Complex 1) [15], diaquabis(3,4-dimethoxybenzoate)bis(nicotinamide)nickel(II) dihydrate (Complex 2) [16], diaquabis(3,4-dimethoxybenzoate)bis(nicotinamide)cobalt(II) dihydrate (Complex 3) [17], were characterized before. Using the crystallographic information files (.cif) of these complexes, Hirshfeld Surface analysis and Molecular Docking Studies were performed. The crystal structures of the complexes were presented in Figure 1.

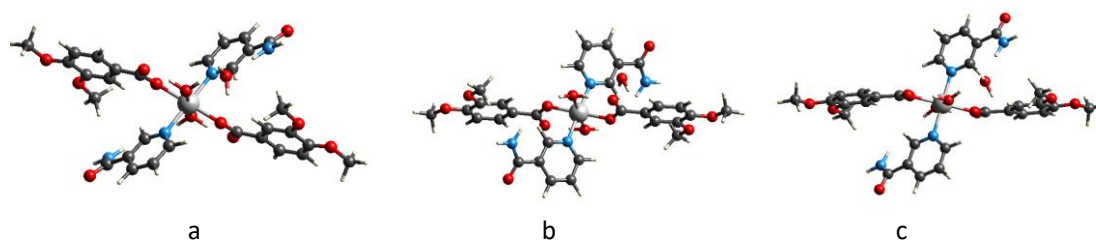


Figure 1. The molecular structures of complex 1 (a), complex 2 (b), and complex 3 (c).

## 2.2. Hirshfeld surface analysis

Hirshfeld surface analysis [19, 20] was performed using CrystalExplorer 21.5 [21] to visualize the complexes' intermolecular interactions. The Hirshfeld surface,  $d_{\text{norm}}$  shape index, curvedness map [21, 22], and 2D fingerprint plots [20] were created using the complexes' crystallographic information file (.cif).

## 2.3. Molecular docking studies

Autodock Vina [23] software was utilized to compute the binding energies of the complexes. The RCSB Protein Data Bank (<https://www.rcsb.org>) was used to download the PDB file of the SARS-CoV-2 main protease enzyme (PDB Code: 7BQY) [24] and the spike protein of the SARS-CoV-2 Omicron variant (PDB Code: 7T9J). Files of ligands with .pdb extension were recorded using cif files of the complexes. The structures of complexes 1-3 are given in Figure 1. The enzyme, which will be modeled, was first optimized with the help of BIOVA Discovery Studio Visualizer 2021 [26] program. The interacting enzyme with the complexes in the active region and ligand-protein interactions were generated using the AutoDockTools 1.5.7 tool [23]. The visualization studies made use of the BIOVA Discovery Studio Visualizer 2021 software.

## 3. Result and discussion

### 3.1. Hirshfeld surface analysis

A molecule's Hirshfeld surface is the area of the crystal where the promolecule's electron density is higher than the procrystal's electron density. Color coding of intermolecular interactions that are shorter (red regions), equal (white regions), or longer (blue regions) than the total of the van der Waals radii is used to produce the Hirshfeld surface. The hydrogen-bonding interactions are indicated by the dark red spots on the Hirshfeld surface mapped on  $d_{\text{norm}}$  (Figures 2a, 3a, and 4a). The existence of interactions like C—H... $\pi$  and  $\pi$ – $\pi$  stacking is confirmed by shape index maps. The neighboring red and blue triangles around the benzene and pyridine rings are compatible with the presence of  $\pi$ – $\pi$  stacking interactions in the structure of the complexes, which contribute greatly to the crystal structure (Figures 2b, 3b, and 4b). The planarity of the aromatic rings is evident in the large green areas and curvedness maps. It is also shown with blue lines that the curvature increases with distance from the regions where the rings are located (Figures 2c, 3c, and 4c).

Because the complexes include a majority of hydrogen, The H...H interactions are the most important interactions (39.0 % (for complex 1), 39.6 % (for complex 2), and 38.9 % (for complex 3) contribution). These interactions appear as high-density and widely dispersed dots on the fingerprint graph. With the tips at  $d_e + d_i = 1.80 \text{ \AA}$ , the pair of

spikes in the fingerprint plot that are identified as  $\text{H}\cdots\text{O}/\text{O}\cdots\text{H}$  interactions have a symmetrical distribution of points (30.0 % contribution for all complexes).  $\text{H}\cdots\text{C}/\text{C}\cdots\text{H}$  interactions resulting from  $\text{C}-\text{H}\cdots\pi$  and  $\pi-\pi$  interactions appear as characteristic pairs of wings in the fingerprint graph, and these interactions contribute 23.2%, 22.6%, and 23.4 to the Hirshfeld surface for complexes 1, 2, and 3, respectively. ( $d_e + d_i = 2.82 \text{ \AA}$ .) All other intermolecular interactions are given in Table 1. Fingerprint graphs are given in Figures 5-7. It was found that these isostructure three complexes contributed similarly to the Hirshfeld surface through intermolecular contacts (Figure 5-7).

The void volumes of complexes 1, 2, and 3 were found  $437.96 \text{ \AA}^3$ ,  $424.50 \text{ \AA}^3$ , and  $428.34 \text{ \AA}^3$ , respectively. The percentages of void volume in the unit cell of complexes 1, 2, and 3 were calculated at 12.98 %, 12.67 %, and 12.73 %, respectively (Figures 2d, 3d, and 4d). This is also consistent with the total energy ranking computed with the B3LYP/6-31G(d,p) basis set. The order is as follows:  $e_{\text{tot}1} > e_{\text{tot}3} > e_{\text{tot}2}$ . The void volume also corresponds to this order.

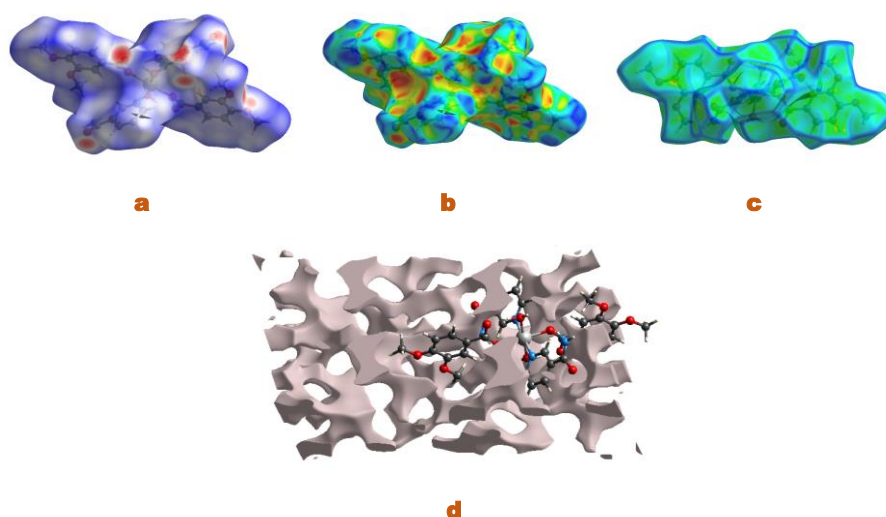


Figure 2.  $D_{\text{norm}}$  map in the range of -0,6759 - 1,3116 a.u (a), shape index (b), curvedness map (c), and void surfaces (d) of complex 1.

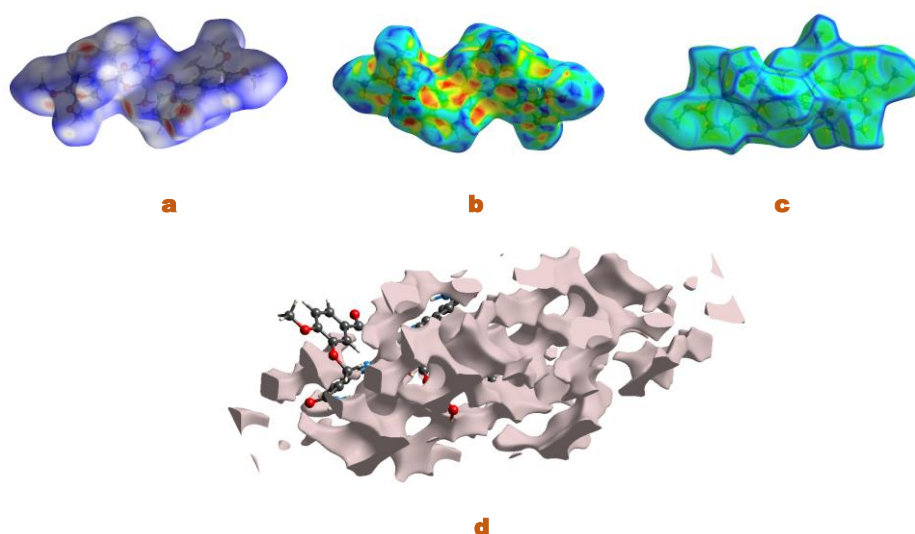


Figure 3.  $D_{\text{norm}}$  map in the range of -0,6660 - 1,3042 a.u (a), shape index (b), curvedness map (c), and void surfaces (d) of complex 2.

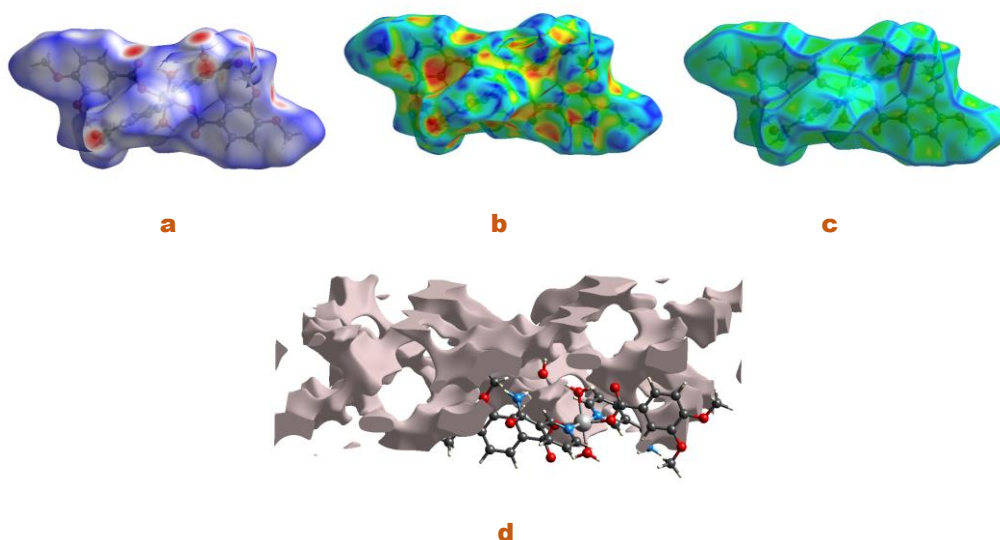


Figure 4.  $D_{\text{norm}}$  map in the range of -0,6722 - 1,3132 a.u (a), shape index (b), curvedness map (c), and void surfaces (d) of complex 3.

Table 1. Intermolecular interaction percentage (%) of the complexes 1-3.

	H... H	H...O/O... H	H...C/C... H	H...N/N... H	C...O/O... C	C...N/N... C	C... C	O... O
<b>Comple x 1</b>	39.0	30.0	23.2	2.3	2.0	0.1	3.2	0.1
<b>Comple x 2</b>	39.6	30.0	22.6	2.1	2.0	0.1	3.32	0.1
<b>Comple x 3</b>	38.9	30.0	23.4	2.3	2.0	0.1	3.2	0.1

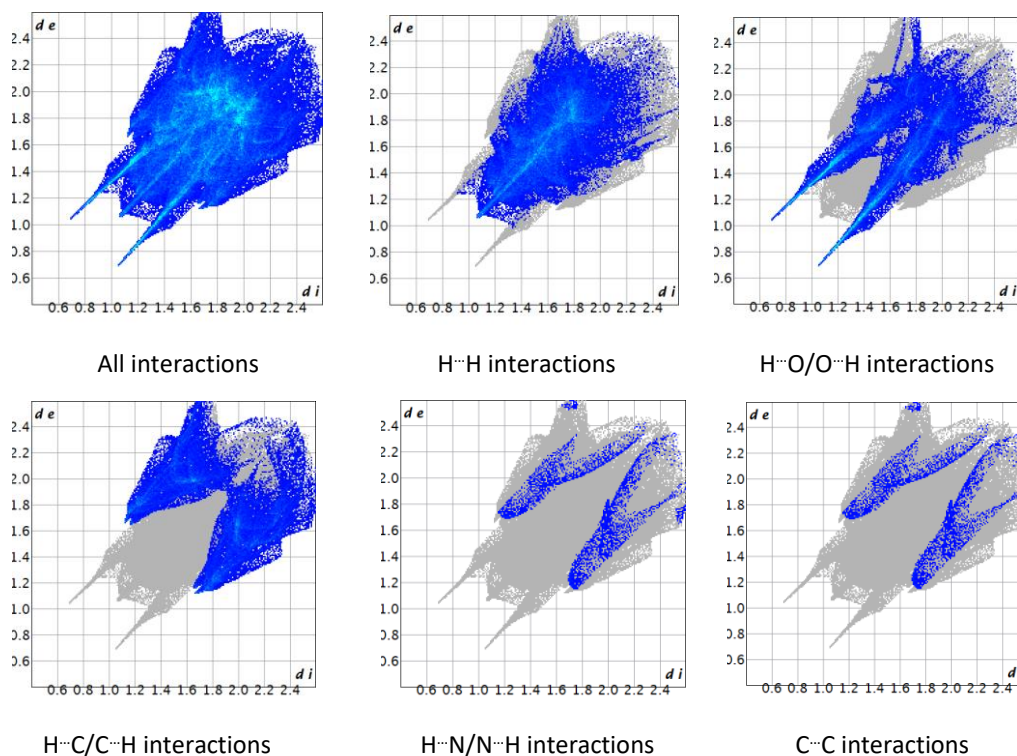


Figure 5. 2D Fingerprint plots of complex 1.

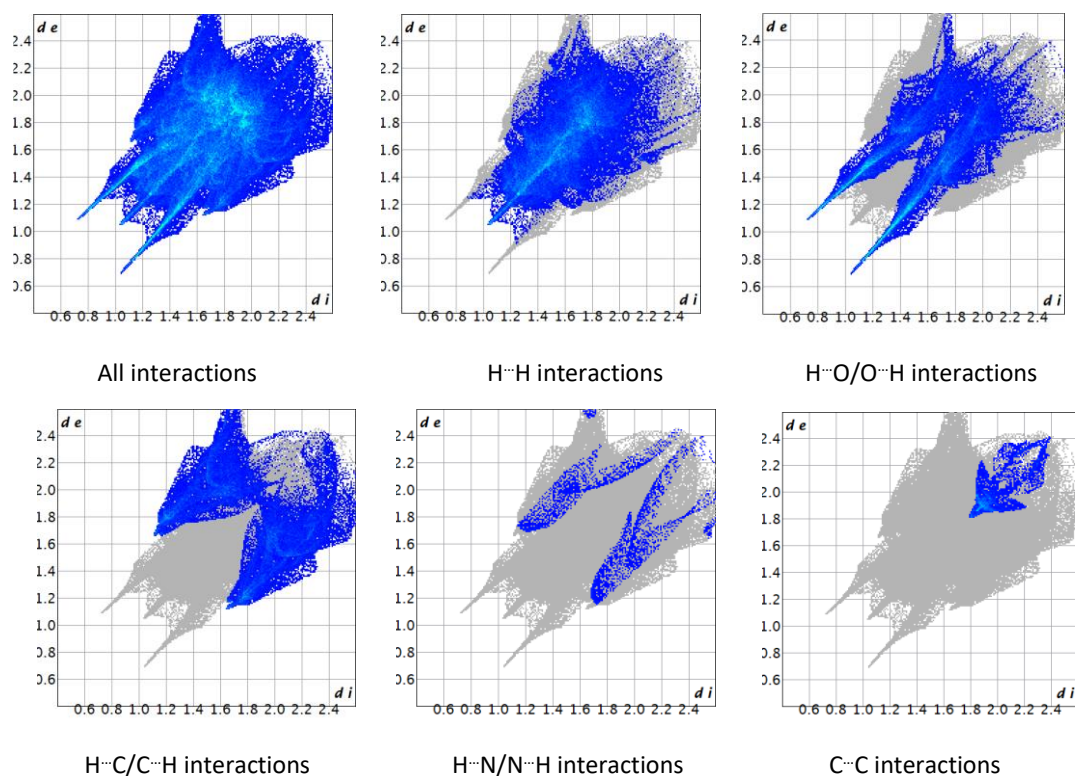


Figure 6. 2D Fingerprint plots of complex 2.

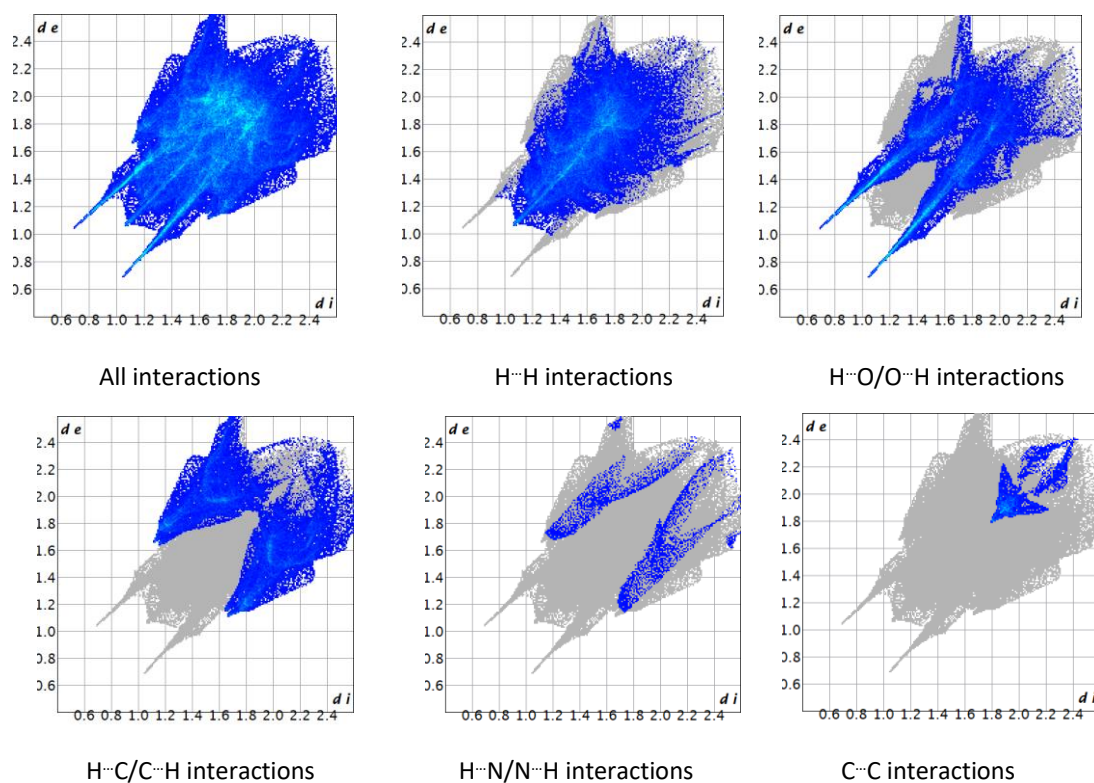


Figure 7. 2D Fingerprint plots of complex 3.

### 3.2. Intermolecular energy calculations

The total energy  $E_{\text{tot}}$  (kJ/mol) is calculated by adding the four main sources of energy: electrostatic ( $E_{\text{ele}}$ ), polarization ( $E_{\text{pol}}$ ), dispersion ( $E_{\text{dis}}$ ), and exchange-repulsion ( $E_{\text{rep}}$ ). The scale factors used are 1.057, 0.740, 0.871, and 0.618 kJ/mol for the B3LYP/6-31G(d,p) electron densities and 1.019, 0.651, 0.901, and 0.811 kJ/mol for the HF/3-21G electron densities, respectively. Since the scale factor is not included in the program for other electron densities, there is no equivalent for the total energy value. As seen in Table 2-4, total energy values are close to each other in B3LYP/6-31G(d,p) and HF/3-21G base sets. For Complex 1, the total energy was calculated as -57.4 and -61.3 kJ/mol in the B3LYP/6-31G(d,p) and HF/3-21G basis sets, respectively. These values were found as -31.9 and -32.6 kJ/mol and -56.0 and -62.0 kJ/mol for complex 2 and complex 3 in B3LYP/6-31G(d,p) and HF/3-21G base sets, respectively. It was determined that the electrostatic, polarization, dispersion, and repulsion energy values in all other basic sets were close to each other. In addition, it was concluded that electrostatic energy contributed the most to the total energy. In structures, hydrogen bondings and weak C-H $\cdots$  $\pi$  contacts make a significant contribution to electrostatic energy.

Table 2. Interaction energy values of the complex 1.

	<b>N</b>	<b>Symop</b>	<b>R</b>	<b>Electron Density</b>	<b>E_ele</b>	<b>E_pol</b>	<b>E_dis</b>	<b>E_rep</b>	<b>E_tot</b>
	1	-	4.39	B3LYP/6-31G(d,p)	-64.9	-14.5	-16.6	59.0	-57.4
	0			HF/6-31G(d,p)	-70.7	-17.2	-16.6	54.3	
	0			DFT/6-31G(d,p)	-64.5	-13.6	-16.6	60.9	
	0			MP2/6-31G(d,p)	-70.7	-17.2	-16.6	54.3	
	0			B3LYP/6-31G(d)	-65.9	-15.2	-16.6	58.3	
	1	-	4.39	HF/6-31G(d)	-71.1	-17.8	-16.6	53.3	
	0			DFT/6-31G(d)	-65.5	-14.4	-16.6	60.3	
	0			MP2/6-31G(d)	-71.1	-17.8	-16.6	53.3	
	1	-	4.39	B3LYP/3-21G	-61.5	-16.3	-16.6	47.6	
	0			HF/3-21G	-68.0	-19.3	-16.6	43.8	-61.3
	0			DFT/3-21G	-60.3	-15.4	-16.6	49.6	
	1	-	4.39	MP2/3-21G	-68.0	-19.3	-16.6	43.8	

Table 3. Interaction energy values of the complex 2.

	<b>N</b>	<b>Symop</b>	<b>R</b>	<b>Electron Density</b>	<b>E_ele</b>	<b>E_pol</b>	<b>E_dis</b>	<b>E_rep</b>	<b>E_tot</b>
	1	-	5.83	B3LYP/6-31G(d,p)	-50.0	-11.8	-9.7	61.6	-31.9
	1	-	5.83	HF/6-31G(d,p)	-55.6	-15.0	-9.7	56.4	
	0			DFT/6-31G(d,p)	-51.7	-11.8	-9.7	63.6	
	0			MP2/6-31G(d,p)	-55.6	-15.0	-9.7	56.4	
	0			B3LYP/6-31G(d)	-50.6	-12.3	-9.7	61.0	

Table 3. (Continued)

1	-	5.83	HF/6-31G(d)	-54.7	-15.1	-9.7	55.4	
0			DFT/6-31G(d)	-47.9	-10.0	-9.7	62.8	
0			MP2/6-31G(d)	-54.7	-15.1	-9.7	55.4	
0			B3LYP/3-21G	-46.7	-13.5	-9.7	55.4	
1	-	5.83	HF/3-21G	-52.4	-17.3	-9.7	50.3	-32.6
0			DFT/3-21G	-40.2	-9.2	-9.7	57.4	
0			MP2/3-21G	-52.4	-17.3	-9.7	50.3	

Table 4. Interaction energy values of the complex 3.

N	Symop	R	Electron Density	E_ele	E_pol	E_dis	E_rep	E_tot
1	-	4.39	B3LYP/6-31G(d,p)	-65.1	-14.5	-16.4	61.2	-56.0
0			HF/6-31G(d,p)	-71.9	-17.7	-16.4	54.8	
0			DFT/6-31G(d,p)	-65.0	-13.7	-16.4	63.2	
0			MP2/6-31G(d,p)	-71.9	-17.7	-16.4	54.8	
0			B3LYP/6-31G(d)	-66.1	-15.2	-16.4	60.6	
0			HF/6-31G(d)	-72.3	-18.2	-16.4	53.9	
0			DFT/6-31G(d)	-65.9	-14.4	-16.4	62.5	
0			MP2/6-31G(d)	-72.3	-18.2	-16.4	53.9	
0			B3LYP/3-21G	-62.4	-16.7	-16.4	49.3	
0			HF/3-21G	-69.3	-19.8	-16.4	44.8	-62.0
0			DFT/3-21G	-61.5	-15.8	-16.4	50.8	
0			MP2/3-21G	-69.3	-19.8	-16.4	44.8	

### 3.3. Molecular docking results

The binding energy between complex 1 and the main protease enzyme was calculated at -7.3 kcal/mol. Complex 1 links the active region of the main protease enzyme of SARS CoV-2 (Mpro) through hydrogen bonds with his41, cys145, his163, ser144, leu141 and thr190,  $\pi$ -anion with glu166, alkyl with leu27, cys145, and pro168 and  $\pi$ -alkyl with his41, cys145, and pro168. The hydrogen bond distances of complex 1 and his41, cys145, his163, ser144, leu141, and thr190 amino acid residues were found as 2.34, 3.59, 2.167, 2.38, 2.08, and 2.25 Å, respectively (Figure 7).

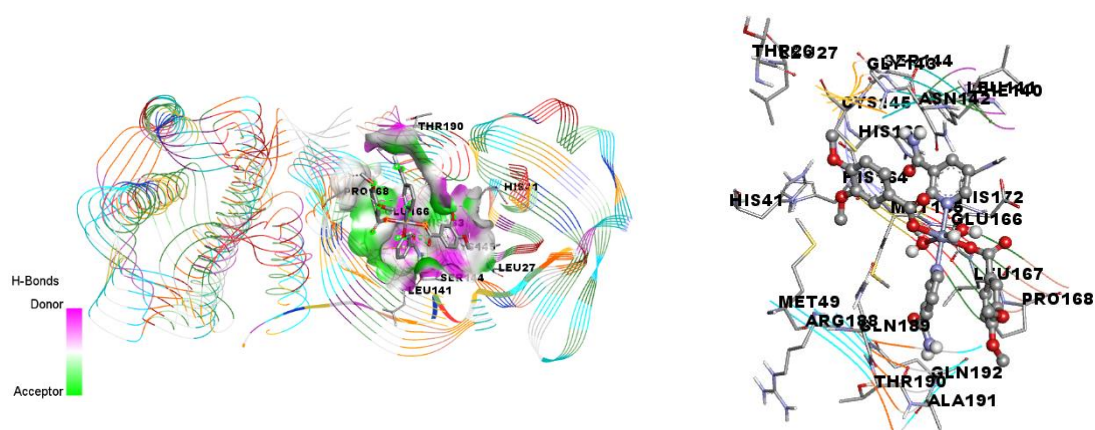


Figure 7. The hydrogen bond interactions between complex 1 and the active region of the Mpro (in left). Two-dimensional interactions of complex 1 with amino acids in the active region of the Mpro (in right).

The binding energy between complex 2 and the Mpro is found as -7.4 kcal/mol. Complex 2 complex interacts active region of the Mpro through hydrogen bonds with his41, ser144, cys145, his163, thr190, and glu166, carbon-hydrogen bond with gln189 and glu166,  $\pi$ -anion with glu166, alkyl with met49 and leu27 and  $\pi$ -alkyl with his41. The hydrogen bond distances of complex 2 and his41, ser144, cys145, his163, thr190, and glu166 amino acid residues were determined as 2.34, 2.81, 3.60, 2.06, 2.21, and 2.20 Å, respectively (Figure 8).

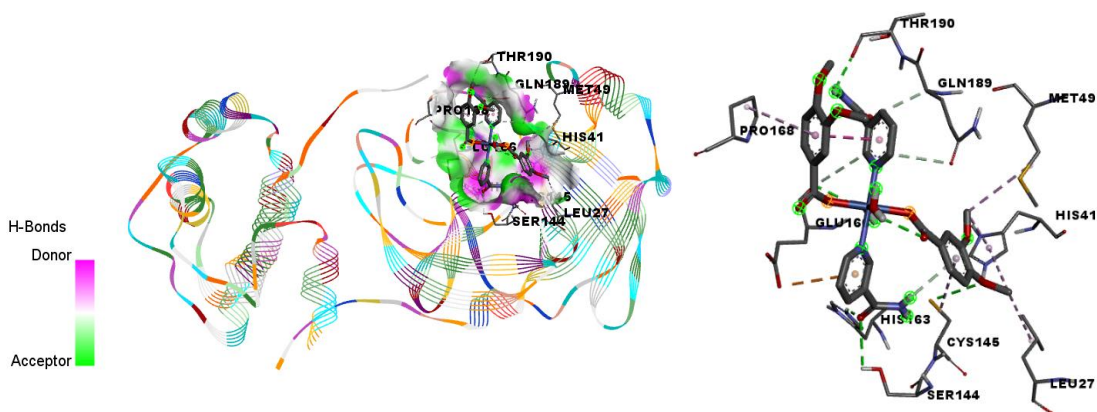


Figure 8. The hydrogen bond interactions between complex 2 and the active region of the Mpro (in left). Two-dimensional interactions of complex 2 with amino acids in the active region of the Mpro (in right).

The binding energy between complex 3 and the Mpro is determined as -7.4 kcal/mol. complex 3 binds the active region of the Mpro via hydrogen bond with thr190, glu166, his41, ser144 cys145 and his163, carbon-hydrogen bond with gln189,  $\pi$ -anion with glu166, alkyl with leu27 and  $\pi$ -alkyl with cys145 pro168, and his41. The hydrogen bond distances of complex 2 and thr190 amino acid residue, glu166, his41, ser144, cys145, and his163 amino acid residues were determined as 2.19, 2.44, 2.33, 2.85, 3.57, and 2.06 Å, respectively (Figure 9).

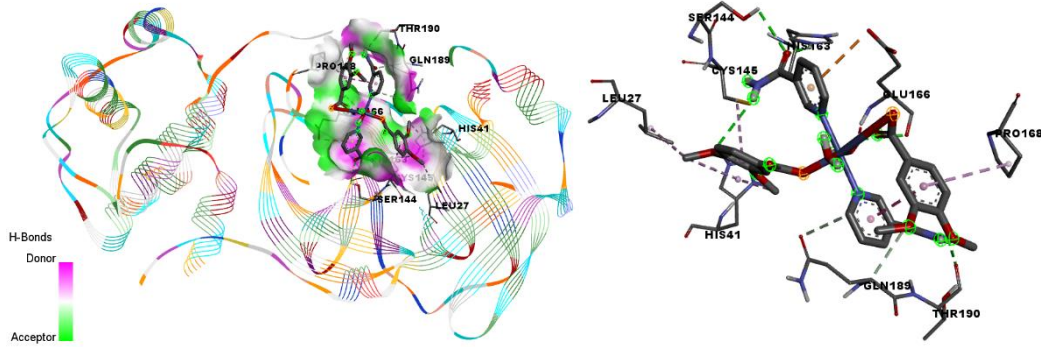


Figure 9. The hydrogen bond interactions between complex 3 and the active region of the Mpro (in left). Two-dimensional interactions of complex 3 with amino acids in the active region of the Mpro (in right).

The binding energy of complex 1 with spike protein of Omicron variant of SARS CoV-2 was determined as -6.6 kcal/mol. Complex 1 interacts active region of the spike protein of Omicron variant of SARS CoV-2 by the hydrogen bond with thr732, val952, and his1058, carbon-hydrogen bond with pro863,  $\pi$ -alkyl with val860, pro862, and pro863. The hydrogen bond distances of complex 1 and thr732, val952, and his1058 amino acid residues were found as 2.65, 2.71, and 2.18 Å, respectively (Figure 10).

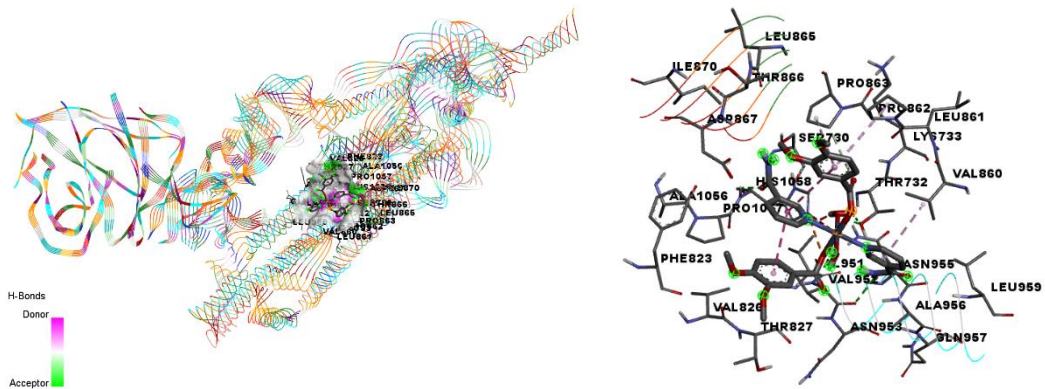


Figure 10. The hydrogen bond interactions between complex 1 and the active region of the spike protein of Omicron variant of SARS CoV-2 (in left). Two-dimensional interactions of complex 1 with amino acids in the active region of the spike protein of Omicron variant of SARS CoV-2 (in right).

The binding energy of complex 2 with spike protein of Omicron variant of SARS CoV-2 was -6.5 kcal/mol. Complex 2 binds to the active region of the spike protein of Omicron variant of SARS CoV-2 via attractive charge with his1058, hydrogen bond with his1058, carbon-hydrogen bond with asp867, pro863 and ala956,  $\pi$ -sigma with val860, alkyl with pro862,  $\pi$ -alkyl with phe823, pro862, and pro863. The hydrogen bond distance between complex 2 and his1058 amino acid residue was found as 2.42 Å (Figure 11).

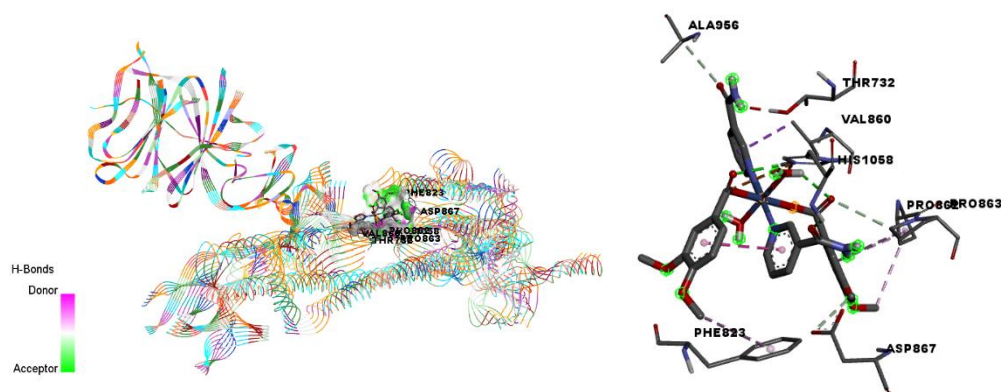


Figure 11. The hydrogen bond interactions between complex 2 and the active region of spike protein of Omicron variant of SARS CoV-2 (in left). Two-dimensional interactions of complex 2 with amino acids in the active region of the spike protein of Omicron variant of SARS CoV-2 (in right).

The binding energy of complex 3 with spike protein of Omicron variant of SARS CoV-2 was calculated at -6.7 kcal/mol. Complex 3 links the active region of the spike protein of Omicron variant of SARS CoV-2 by attractive charge with his1058, hydrogen bond with his1058, carbon-hydrogen bond with thr827, pro863, and val826,  $\pi$ -sigma with val952, alkyl with pro862,  $\pi$ -alkyl with phe823, ala956, pro1057, and val860. The distance of the hydrogen bond between complex 3 and his1058 amino acid residue was found as 2.32 Å (Figure 12).

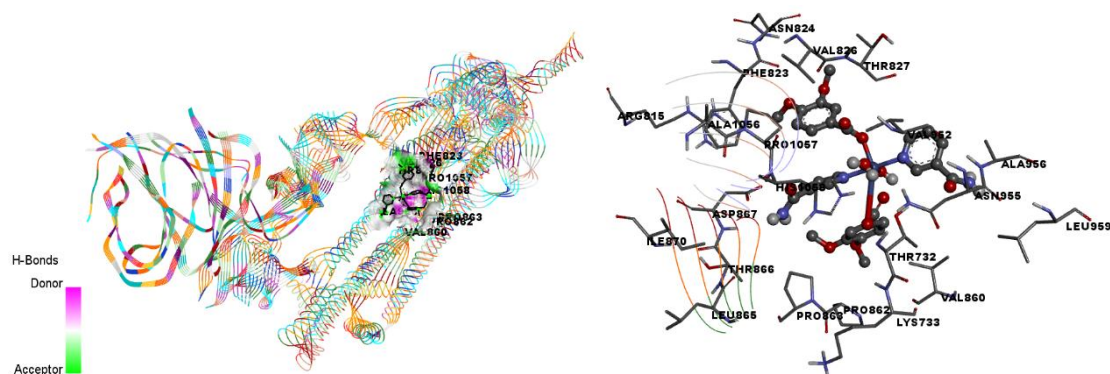


Figure 12. The hydrogen bond interactions between complex 3 and the active region of spike protein of Omicron variant of SARS CoV-2 (in left). Two-dimensional interactions of complex 3 with amino acids in the active region of the spike protein of Omicron variant of SARS CoV-2 (in right).

#### 4. Conclusion

In this study, Hirshfeld Surface Analysis findings revealed that  $H\cdots O/O\cdots H$ ,  $C\cdots O/O\cdots C$ ,  $H\cdots H$ ,  $H\cdots N/N\cdots H$ ,  $H\cdots C/C\cdots H$ , and  $C\cdots N/N\cdots C$ ,  $O\cdots O$  and  $C\cdots C$  interactions were observed on the Hirshfeld surface of diaquabis(3,4-dimethoxybenzoate)bis(nicotinamide)zinc(II) dihydrate, diaquabis(3,4-dimethoxybenzoate)bis(nicotinamide)nickel(II) dihydrate, diaquabis(3,4-dimethoxybenzoate)bis(nicotinamide)cobalt(II) dihydrate.  $H\cdots H$  interactions provide the most important contribution to the Hirshfeld surface of the

complexes. H<sup>⋯</sup>O/O<sup>⋯</sup>H interactions, which support the existence of hydrogen bonds in structures, also make the second most important contribution. The results of the Hirshfeld surface analysis revealed that the complexes can make many non-covalent interactions, and it is thought that these interactions may contribute to the stability of the crystal package. By finding the donor-acceptor sites that allow the molecules to interact with the protein, it is possible to do some *in silico* experiments to assess if they may be utilized as drugs in the cure of certain diseases. In this context, the interactions of the complexes with the main protease enzyme and spike protein of Omicron variant SARS CoV-2 were investigated *in silico*. When the structure-activity relationship of the complexes was evaluated, it was determined that there were differences between the results regarding the binding energies. Several interactions, including attractive charges, hydrogen bonds, carbon-hydrogen bonds,  $\pi$ -sigma,  $\pi$ -anion,  $\pi$ -alkyl, and alkyl interactions, have been detected between the complexes and Mpro enzyme and spike protein of coronavirus. Considering the variety of binding energy and interaction types, it is thought that *in vitro/in vivo* experiments can be performed for complex 3, and promising results will be obtained.

## References

- [1] Cramer, C.J., **Essentials of computational chemistry: theories and models**. Wiley, Chichester, West Sussex, England ; Hoboken, NJ, (2004).
- [2] Jensen, F., **Introduction to computational chemistry**. John Wiley & Sons, Chichester, UK ; Hoboken, NJ, (2017).
- [3] Lin, Z., Interplay between Theory and Experiment: Computational Organometallic and Transition Metal Chemistry. **Accounts of Chemical Research**, 43, 602–611, (2010). <https://doi.org/10.1021/ar9002027>
- [4] Spackman, M.A., Jayatilaka, D., Hirshfeld surface analysis, **CrystEngComm**, 11, 19–32, (2009). <https://doi.org/10.1039/B818330A>
- [5] Spackman, M.A., Spackman, P.R., Thomas, S.P., 13 Beyond Hirshfeld surface analysis: Interaction energies, energy frameworks and lattice energies with CrystalExplorer. In: 13 Beyond Hirshfeld surface analysis: Interaction energies, energy frameworks and lattice energies with CrystalExplorer. pp. 329–352. De Gruyter, (2021).
- [6] McKinnon, J.J., Jayatilaka, D., Spackman, M.A., Towards quantitative analysis of intermolecular interactions with Hirshfeld surfaces, **Chemical Communications**, 3814, (2007). <https://doi.org/10.1039/b704980c>
- [7] McKinnon, J.J., Fabbiani, F.P.A., Spackman, M.A., Comparison of Polymorphic Molecular Crystal Structures through Hirshfeld Surface Analysis, **Crystal Growth & Design**, 7, 755–769, (2007). <https://doi.org/10.1021/cg060773k>
- [8] Vijesh, A.M., Isloor, A.M., Telkar, S., Arulmoli, T., Fun, H.-K., Molecular docking studies of some new imidazole derivatives for antimicrobial properties. **Arabian Journal of Chemistry**, 6, 197–204, (2013). <https://doi.org/10.1016/j.arabjc.2011.10.007>
- [9] Shoichet, B.K., McGovern, S.L., Wei, B., Irwin, J.J., Lead discovery using molecular docking, **Current Opinion in Chemical Biology**, 6, 439–446, (2002). [https://doi.org/10.1016/S1367-5931\(02\)00339-3](https://doi.org/10.1016/S1367-5931(02)00339-3)
- [10] Jain, S., Potschka, H., Chandra, P.P., Tripathi, M., Vohora, D., Management of COVID-19 in patients with seizures: Mechanisms of action of potential COVID-19 drug treatments and consideration for potential drug-drug interactions with

- anti-seizure medications, **Epilepsy Research**, 174, 106675, (2021). <https://doi.org/10.1016/j.eplepsyres.2021.106675>
- [11] Cheke, R.S., The Molecular Docking Study of Potential Drug Candidates Showing Anti-COVID-19 Activity by Exploring of Therapeutic Targets of SARS-CoV-2, **The Eurasian Journal of Medicine and Oncology (EJMO)**, (2020). <https://doi.org/10.14744/ejmo.2020.31503>
- [12] Singh, S., Florez, H., Coronavirus disease 2019 drug discovery through molecular docking, **F1000Research**, 9, 502, (2020). <https://doi.org/10.12688/f1000research.24218.1>
- [13] Parmar, G., Shah, A., Shah, S., Seth, A.K., Identification of bioactive phytoconstituents from the plant *euphorbia hirta* as potential inhibitor of sars-cov-2: An in-silico approach, **Biointerface Research in Applied Chemistry**, 1385–1396, (2022).
- [14] Daoud, S., Alabed, S.J., Dahabiyeh, L.A., Identification of potential COVID-19 main protease inhibitors using structure-based pharmacophore approach, molecular docking and repurposing studies, **Acta Pharmaceutica**. 71, 163–174 (2021). <https://doi.org/10.2478/acph-2021-0016>
- [15] Kaya, A.A., Demircioğlu, Z., Kaya, E.Ç., Büyükgüngör, O., Synthesis, X-ray structural characterization, NLO, MEP, NBO and HOMO-LUMO analysis using DFT study of Zn(II)bis(3,4 dimethoxybenzoate)bis(nicotinamide) dihydrate, **Heterocyclic Communications**, 20, 51–59, (2014). <https://doi.org/10.1515/hc-2013-0160>
- [16] Kaya, E.Ç., Kaya, A.A., Demircioğlu, Z., Büyükgüngör, O., Synthesis, spectroscopic characterization, X-ray structure and DFT calculations of Ni(II)bis(3,4 dimethoxybenzoate)bis(nicotinamide) dihydrate, **Heterocyclic Communications**, 23, 115–123, (2017). <https://doi.org/10.1515/hc-2016-0099>
- [17] Kaya, A.A., Demircioğlu, Z., Kaya, E.Ç., Büyükgüngör, O., Synthesis, X-ray structural characterization, NLO, MEP, NBO and HOMO-LUMO analysis using DFT study of Zn(II)bis(3,4 dimethoxybenzoate)bis(nicotinamide) dihydrate, **Heterocyclic Communications**, 20, 51–59, (2014). <https://doi.org/10.1515/hc-2013-0160>
- [18] Spackman, M.A., Jayatilaka, D., Hirshfeld surface analysis, **CrystEngComm**, 11, 19–32, (2009). <https://doi.org/10.1039/B818330A>
- [19] Hirshfeld, F.L.: Bonded-atom fragments for describing molecular charge densities. *Theoret. Chim. Acta*. 44, 129–138 (1977). <https://doi.org/10.1007/BF00549096>
- [20] Spackman, M.A., Jayatilaka, D., Hirshfeld surface analysis, **CrystEngComm**, 11, 19–32, (2009). <https://doi.org/10.1039/B818330A>
- [21] Spackman, P.R., Turner, M.J., McKinnon, J.J., Wolff, S.K., Grimwood, D.J., Jayatilaka, D., Spackman, M.A., CrystalExplorer: a program for Hirshfeld surface analysis, visualization and quantitative analysis of molecular crystals, **Journal of Applied Crystallography**, 54, 1006–1011, (2021). <https://doi.org/10.1107/S1600576721002910>
- [22] McKinnon, J.J., Jayatilaka, D., Spackman, M.A., Towards quantitative analysis of intermolecular interactions with Hirshfeld surfaces, **Chemical Communications**, 3814–3816, (2007). <https://doi.org/10.1039/b704980c>
- [23] Trott, O., Olson, A.J., AutoDock Vina: Improving the speed and accuracy of docking with a new scoring function, efficient optimization, and multithreading, **Journal of Computational Chemistry**, 31, 455, (2009). <https://doi.org/10.1002/jcc.21334>

- [24] Fakhar, Z., Khan, S., AlOmar, S.Y., Alkhuriji, A., Ahmad, A., ABBV-744 as a potential inhibitor of SARS-CoV-2 main protease enzyme against COVID-19, **Scientific Reports**, 11, 234, (2021). <https://doi.org/10.1038/s41598-020-79918-3>
- [25] Bank, R.P.D., RCSB PDB - 7T9J: Cryo-EM structure of the SARS-CoV-2 Omicron spike protein, <https://www.rcsb.org/structure/7T9J>
- [26]. BIOVIA, Dassault Systèmes, BIOVA Discovery Studio Visualizer 2021, v21.1.0.20298, San Diego: Dassault Systèmes, (2021).